JOURNAL OF GEOPHYSICAL RESEARCH, VOL. ???, XXXX, DOI:10.1029/,

Determining the contribution of volcanic ash and Boundary Layer aerosol in backscatter lidar returns: a three-component atmosphere approach

Franco Marenco[1] and Robin J. Hogan[2]

Submitted on 3 December 2010 to JGR special section "The Eyjafjallajkull Volcanic Eruption in 2010"

[1]Observational Based Research, Met Office, United Kingdom

[2]Department of Meteorology, University of Reading, United Kingdom

Abstract. A solution of the lidar equation is dicussed, that permits combining backscatter and depolarisation measurements to quantitatively distinguish two different aerosol types with different depolarisation properties. The method has been successfully applied to simultaneous observations of volcanic ash and Boundary Layer aerosol obtained in Exeter, United Kingdom, on 16 and 18 April 2010, permitting to quantify the contribution of the two aerosols separately. First a subset of the atmospheric profiles is used where the two aerosol types belong to clearly distinguished layers, for the purpose of characterising the ash in terms of lidar ratio and depolarisation. These quantities are then used in a three-component atmosphere solution scheme of the lidar equation applied to the full dataset, in order to compute the extinction coefficient of both aerosol types separately. On 16 April a thin ash layer, 100–400 m deep, is observed (average and maximum estimated ash optical depth: 0.11 and 0.2); it descends from $\sim$ 2800 to $\sim$ 1400 m altitude in a 6-hour time. On 18 April a double ash layer, $\sim$ 400 m deep, is observed just above the morning Boundary Layer (average and maximum estimated ash optical depth: 0.19 and 0.27). In the afternoon this layer is entrained into the Boundary Layer mixing, reaching a depth of $\sim$ 1800 m (average and maximum estimated ash optical depth: 0.1 and 0.15). An additional ash layer, with very small optical depth, has been observed on 18 April at an altitude of 3500–4000 m. The observations seem to suggest approximate peak ash concentrations of $\sim$ 1500 and $\sim$ 1000 μg/m^3, respectively, on the two observations dates.

1. Introduction

The April–May 2010 eruption of the Eyjafjallajökull, Iceland, happened during a period characterised by high atmospheric pressures over Northern Europe and the North Atlantic [*Petersen*, 2010]. This resulted into long-range transport of the volcanic ash plumes to Northern, Central and Southern Europe and to the Atlantic Ocean, with atmospheric residence times of the order of several days. A major air traffic disruption happened as a consequence of this [*Gertisser*, 2010]. Observations carried out during that period are of great interest for the validation and improvement of numerical dispersion models used for the prediction of volcanic ash concentrations. They have moreover proven to be a a useful tool in the nearly real-time decision-making process concerning the opening or closure of airspace. Lidar has been one of the most successful remote-sensing intruments for locating the plumes: several ground-based stations have carried out observations [*Mona et al.*, 2010; *Ansmann et al.*, 2010; *Flentje et al.*, 2010; *Pietruczuk et al.*, 2010; *Hogan et al.*, 2010] and moreover observations of volcanic ash have also been obtained by airborne lidar [*Schumann et al.*, 2010]. **[ADD MORE CITATIONS AS WE PROGRESS ON THE AIRBORNE DATASET]**

Several papers have appeared in the last decades discussing the solution to the lidar equation; see e.g. *Fernald et al.* [1972]; *Fernald* [1984]; *Klett* [1985]; *Kovalev* [1993]; *Takamura et al.* [1994]; *Marenco et al.* [1997]; *Hogan et al.* [2010]. This amount of literature is justified by the fact that the equation is underdetermined, i.e. for any measured lidar profile infinite mathematical solutions are possible, whereas of course only one of them will have to be retained as the best estimate of the state of the atmosphere. In the

assumption of single elastic scattering, monochromatic radiative transfer applied to lidar returns leaves us with backscatter and extinction tied together in an integral equation: with two unknowns and only one equation, insufficient information is available for finding a deterministic solution.

In the absence of a definite physical principle to be used for the purpose of constraining the solution, since *Fernald et al.* [1972] the scientific community has often resorted to the assumption that the lidar ratio (extinction-to-backscatter ratio) is constant. This assumption could in principle be relaxed as in *Klett* [1985] provided that the vertical profile of the lidar ratio is known, but if one is left with an elastic backscatter lidar alone there is of course no simple way of establishing that profile. Note that on one side the assumption of a constant lidar ratio is made because there are often no other practical possibilities for inverting the lidar equation, and on the other side this seems a reasonable assumption for an aerosol layer from a given source and for which microphysical properties such as composition and particle size/shape may be assumed homogeneous.

Even in the assumption of a constant lidar ratio, the lidar retrieval remains underdetermined since two parameters need be set: one of them is the value of the lidar ratio itself, and the other is the lidar calibration constant; the latter is usually determined by comparison of the signal with what is expected from a known target, most often Rayleigh scattering by an aerosol-free layer: this framework is often referred to as the Fernald-Klett approach [*Fernald*, 1984; *Klett*, 1985]. The lidar constant is usually not determined *a priori* in the laboratory, for two reasons: the first being that the laser output and receiver efficiency may vary (i.e. the lidar constant is so called because of its independence upon range, but it still may vary with time), and the second, more fundamental, is that as

shown by *Fernald* [1984] the mathematical solution is unstable for a near-range calibration, so that the reference range used for calibration must be taken at the far end of the lidar profile.

Note that the Fernald-Klett approach is not the only one that is based on the assumption of a constant lidar ratio. Two independent constrains to the lidar equation must still be given (this being required mathematically), and several approaches have appeared in the literature. *Kovalev* [1993], for instance, proposes a solution based on the knowledge of the lidar ratio and of the aerosol optical depth; *Di Girolamo et al.* [1994] use a solution based on *two* aerosol-free calibration ranges, one below and one above the aerosol layer; and *Takamura et al.* [1994]; *Marenco et al.* [1997] propose a solution based on an independent optical depth measurement and an aerosol-free calibration range.

All the solutions to the lidar equation mentioned above are based on a two-component atmosphere, where the components are the molecular free-atmosphere (Rayleigh scattering) and the aerosols, respectively; the first component being assumed to be fully known from a model or a radiosonde profile, and the second component being assumed to have rather homogeneous properties (lidar ratio). If distinct aerosol layers are observed at the same time, which are believed to have different properties, a two-component scheme can still be used by dividing up the lidar profiles into separate sections. This approach will however be insufficient for cases when two different aerosol types co-exist in a same atmospheric layer: if knowing in advance how the proportion of the two aerosols varies with range, one could use one of the schemes that assumes a variable lidar ratio, but this cannot be expected to work if that proportion has to be determined from the lidar observations.

The addition of a depolarisation channel has proven in many cases to be the most reliable way to distinguish volcanic ash from other, more common, aerosols, and a strong depolarisation is considered a good tracer for ash. In particular, the observed ash layers have sometimes been observed at a sufficiently high altitude, well above the Boundary Layer (BL) aerosol, and thus could be separately treated. At other times, however, the ash has been reaching the BL top, and as a consequence has been mixing with the BL aerosol. In such observations, the lidar signal can be inverted into quantitative measurements (extinction coefficient), and the depolarisation signal can be separately used as a qualitative information useful to distinguish the ash from the BL aerosol background, but working within a two-component atmosphere framework it may be difficult in some scenes to quantify the contribution of both aerosol types separately.

This paper originates from the remark that if depolarisation is good at identifying the contribution of ash rather than more common aerosols, then the depolarisation information should be incorporated into the aerosol inversion scheme. As a matter of fact, having a depolarisation lidar channel permits having an additional and independent equation, and thus permits including additional unknowns to the lidar problem. We take this opportunity for experimenting a three-component atmosphere reduction scheme, where the three components will be, respecively: Rayleigh scattering, volcanic ash (depolarising), and common aerosols (non-depolarising).

Section 2 shortly describes the origin of the data and recalls the preliminary standard depolarization lidar processing that is applied throughout this article; section 3 momentarily treats selected lidar profiles, where ash is well distinct from other aerosols, in a two-component atmosphere scheme, for the purpose of characterizing volcanic ash in terms of

lidar ratio and depolarisation ratio; section 4 illustrates the mathematical details of the three-component atmosphere approach; and section 5 presents its application and results. Finally, section 6 presents a discussion on the observations and some conclusions.

2. Range-corrected signal and volume depolarisation ratio

Ground-based elastic backscattering lidar measurements have been taken at Exeter (50°44′N, 3°29′W, 30 m-AMSL) on 15–18 April 2010, in an effort to observe the volcanic ash plume caused by the eruption of the Eyjafjallajökull; the measurements were interrupted on the evening of the 18th as the lidar was to be fitted to our research aircraft, where it belongs. Volcanic ash layers have been identified mostly on 16 and 18 April, and discussion in this paper will focus on these two observation days for the purpose of illustrating the three-component approach.

The lidar system used is an ALS450 manufactured by Leosphere, operating at 355 nm and featuring a depolarisation channel. Measurements were taken with a vertical resolution of 1.5 m and an integration time of 20 s, but vertical smoothing with a running average and additional integration were applied during the post-processing in order to reduce the signal-to-noise ratio. Data presented here thus have a vertical resolution of 45 m and an integration time of 1 min, except for section 3 where the data presented will exceptionally have an integration time of 5 min. Please note that local time (LT) is used throughout this paper (British summer time, UTC+1). Full overlap of the receiver field-of-view with the emitted beam is achieved at a range of 300 m, and only data beyond this point will be considered here.

The treatment of depolarisation lidar data is explained in detail in *Freudenthaler et al.* [2009]. After background subtraction and range-correction, the first step in the data

treatment is the calibration of the depolarisation ratio, which we do on a profile-by-profile basis in an aerosol-free region, by comparison with the depolarisation of molecular scattering. This calibration permits the determination of $K^* = K^{\perp}/K^{\parallel}$, the ratio of the non-depolarised channel ($\parallel$) lidar constant to the depolarised channel ($\perp$) lidar constant. Once this is done, it is possible to determine the range-corrected signal:

$$P = P^{\parallel} + \frac{P^{\perp}}{K^*} \tag{1}$$

and the volume depolarisation ratio:

$$D = \frac{P^{\perp}}{K^* P^{\parallel}} \ , \tag{2}$$

where $P^{\parallel}$ and $P^{\perp}$ are the range-corrected lidar signals for each of the two detection channels. Whatever aerosol inversion scheme is to be used, it is most accurate to use the combined channel range-corrected signal in Eq. (1) rather than $P^{\parallel}$ alone.

In a real lidar system, account for the cross-talk between the channels must be made, and in particular for parallel-polarised light entering the depolarised channel. This can be achieved by substituting $P^{\perp}$ in the above with $P_1^{\perp} = P^{\perp} - \gamma K^* P^{\parallel}$, where γ is the cross-talk. The calibration constant is to be computed as:

$$K^* = \frac{P_c^{\perp}}{P_c^{\parallel}(\delta_m + \gamma)}, \tag{3}$$

where $P_c^{\parallel}$ and $P_c^{\perp}$ refer to the measured range-corrected signals in a molecular portion of the profile used for calibration, and δ_m is the molecular depolarisation ratio. An extensive treatment of the channel cross-talk in depolarisation lidar can be found in *Freudenthaler et al.* [2009], where more general equations are given. For our lidar, it is estimated that $\gamma = 0.025$.

The value of δ_m is extensively discussed in *Behrendt and Nakamura* [2002], and is dependent upon the receiver bandwith. For the Leosphere lidar, the latter is 28.6 cm^{-1} (0.36 nm), and by interpolating the values given in that article, $\delta_m = 0.00415$. As we can see, $\delta_m \ll \gamma$, and the calibration in Eq. (3) is therefore controlled by the cross-talk more than by δ_m.

The range-corrected signal and the volume depolarisation ratio for the 16 and 18 April are depicted in Fig 1 and 2. The following features are observed in the lidar range-corrected signal for 16 April: aerosol in the BL (up to 1000–1500 m); broken low level clouds between 11:00 and 18:00 LT; and a layer at higher altitude, starting at 14:00 LT a little lower than 3000 m, and slowly descending down to just above the BL. Vertical profiles featuring clouds have been screened out in the bottom panel, since we want to focus on aerosol retrievals only. As it can be observed from the bottom panel, the higher aerosol layer features a marked volume depolarisation ratio, absent for the BL aerosol layer. We believe this signature to indicate its nature to be volcanic ash, and will therefore denote it as such in what follows.

The 18 April data can be similarly examined from these qualitative plots. We notice a low BL height at the start of the day, rising up to $\sim$ 1700 m in the late afternoon, with formation of a low-level cloud for a short period around 19:00 LT. Signal from a depolarising ash layer just above the BL is detectable in the morning until 14:00 LT, but as the BL top rises the ash loses its identity and is entrained in the BL by turbulent mixing; the signature of the mixing is clearly seen from the depolarisation panel between 14:00 and 18:00 LT. A weakly depolarising layer is also observed for the whole duration

of the observations at 3500–4000 m: we also believe this layer to be ash, but in a much smaller concentration.

3. Characterization of volcanic ash

In this section, we characterize volcanic ash in terms of lidar ratio and aerosol depolarisation ratio, as these quantities will be needed for the three-component atmosphere method. Characterization of the volcanic ash is best carried out by selecting those profiles where the ash layer yields a significant lidar signal and is at the same time clearly distinct from the BL aerosol.

For this purpose, 48 profiles with a 5 min integration time have been selected from the 16 April dataset; for the selected profiles no cloud disturbance is detected, and the ash layer is well above the BL aerosol, separated by what appears to be a purely molecular layer. The latter circumstance permits determining the optical depth of the ash layer by normalising the lidar signal to Rayleigh scattering below and above the layer, as in *Di Girolamo et al.* [1994]. In this way the two-component atmosphere lidar equation is fully constrained, so that the lidar ratio and the atmospheric profiles can be fully determined. In order to do this we use the equations outlined in *Marenco et al.* [1997], with the difference that we are using the layer optical depth that we have determined from the lidar profile, instead of a measured optical depth from a sun-photometer.

Once the extinction and backscatter profiles are known, we determine the aerosol depolarisation ratio as in *Freudenthaler et al.* [2009, section 2.3]. We extract a per-profile average ash depolarisation ratio by averaging the aerosol depolarisation ratio over the portion of the ash layer with extinction coefficient larger than half the profile maximum. At the end of this procedure, we are left with one value for the ash depolarisation ratio

and one for the lidar ratio for every profile. The distribution of this data is illustrated in Fig. 3. The mean lidar ratio over the 48 elements is 82 sr (median 80 sr, standard deviation 15 sr) and the mean depolarisation ratio is 0.342 (median 0.344, standard deviation 0.046). As the data are evenly spread around their average, we shall assume the latter as being representative of volcanic ash for the purpose of this article.

4. Three-component atmosphere approach

As mentioned in the introduction, we propose a solution of the lidar equation based on three distinct atmospheric components: aerosol types 1 and 2 plus the molecular contribution m. The two aerosol types are to be distinguished based on depolarisation. The equations for the range-corrected lidar signal and the volume depolarisation ratio can be written as follows:

$$P = K' \left(\beta_1 + \beta_2 + \beta_m\right) e^{-2\int_{R_c}^{R}(\alpha_1+\alpha_2+\alpha_m)dR} \tag{4}$$

$$D = \frac{\frac{\delta_1\beta_1}{1+\delta_1} + \frac{\delta_2\beta_2}{1+\delta_2} + \frac{\delta_m\beta_m}{1+\delta_m}}{\frac{\beta_1}{1+\delta_1} + \frac{\beta_2}{1+\delta_2} + \frac{\beta_m}{1+\delta_m}} , \tag{5}$$

where $K' = K^{\|} e^{-2\int_0^{R_c}(\alpha_1+\alpha_2+\alpha_m)dR}$ is an unknown calibration parameter, R_c is a calibration range where we assume the state of the atmosphere to be known (usually molecular), β_i denotes the backscattering coefficient, α_i denotes the extinction coefficient, δ_i denotes the aerosol or molecular depolarisation ratio, and $i = 1, 2, m$ denotes the atmospheric component. Normalisation of the contribution of each atmospheric component by $1 + \delta_i$ in both the numerator and denominator of Eq. (5) can be easily understood by recalling that $\delta_i = \beta_i^{\perp}/\beta_i^{\|}$ and $\beta_i = \beta_i^{\|} + \beta_i^{\perp}$.

We shall assume β_m, α_m and δ_m to be fully known (see *Behrendt and Nakamura*, 2002 for a characterisation of δ_m), and that the two aerosol types each have a known lidar ratio

$S_i = \alpha_i/\beta_i$ and a known aerosol depolarisation ratio δ_i. In principle, all equations in this section could also be used with δ_1, δ_2, S_1 and S_2 being known functions of range and time, although there is no obvious method to determine those functions and thus for practical reasons we will use constants when applying the inversion scheme. As we are interested in dealing with a depolarising (ash) and a non-depolarising aerosol (BL), we shall assume in the following that $\delta_1 \neq 0$ and $\delta_2 = 0$, but similar (just more cumbersome) equations could be developed for the more general case, provided that $\delta_1 \neq \delta_2$. No restrictions apply to S_1 and S_2, so that they can possibly be equal. From Eq. (5):

$$\beta_2 = \frac{\left(\frac{\delta_m}{D} - 1\right)\beta_m}{1+\delta_m} + \frac{\left(\frac{\delta_1}{D} - 1\right)\beta_1}{1+\delta_1} \tag{6}$$

and by variable substitution in Eq. (4):

$$P = K'\left(\beta'_m + \epsilon\beta_1\right) e^{-2\int_{R_c}^{R}(\alpha'_m + \eta\beta_1)dR}\,, \tag{7}$$

where the following can be computed from the measured volume depolarisation ratio D, and are fully known functions of range:

$$\beta'_m = \beta_m\left[1 + \frac{\frac{\delta_m}{D} - 1}{1+\delta_m}\right] \tag{8}$$

$$\alpha'_m = \alpha_m + S_2\,\beta_m\,\frac{\frac{\delta_m}{D} - 1}{1+\delta_m} \tag{9}$$

$$\epsilon = 1 + \frac{\frac{\delta_1}{D} - 1}{1+\delta_1} \tag{10}$$

$$\eta = S_1 + S_2\,\frac{\frac{\delta_1}{D} - 1}{1+\delta_1}\,. \tag{11}$$

With Eq. (7) we have reduced the problem to a single integral equation, with the unknown being $\beta_1(R)$; K' is an additional unknown parameter that will need setting through a boundary condition (signal normalisation at the calibration range). We note that this equation is very similar to the two-component atmosphere lidar equation, and

we apply to it a resolving scheme similar to the one described by *Fernald et al.* [1972]. We define:

$$X_1 = e^{-2\int_{R_c}^{R} \eta\beta_1 dR} \tag{12}$$

and

$$X_m = e^{-2\int_{R_c}^{R} \alpha'_m dR} \tag{13}$$

so that Eq. (7) can be rewritten as a linear first order differential equation:

$$\frac{dX_1}{dR} - \frac{2\eta\beta'_m}{\epsilon} X_1 = -\frac{2\eta P}{\epsilon K' X_m} , \tag{14}$$

and:

$$\beta_1 = -\frac{1}{2\eta X_1}\frac{dX_1}{dR} = \frac{1}{\epsilon}\left(\frac{P}{K' X_m X_1} - \beta'_m\right) . \tag{15}$$

If we now assume that we fully know the state of the atmosphere at the calibration range R_c:

$$K' = \frac{P_c}{\beta'_{mc} + \epsilon_c \beta_{1c}} , \tag{16}$$

where $P_c = P(R_c)$, $\beta'_{mc} = \beta'_m(R_c)$, $\beta_{1c} = \beta_1(R_c)$, $\epsilon_c = \epsilon(R_c)$, and $X_m(R_c) = X_1(R_c) = 1$.

The solution of Eq. (14) is as follows:

$$X_1 = e^{2\int_{R_c}^{R} \frac{\eta\beta'_m}{\epsilon} dR} \left\{1 - \frac{2}{K'}\int_{R_c}^{R} \frac{\eta P}{\epsilon X_m} e^{-2\int_{R_c}^{R} \frac{\eta\beta'_m}{\epsilon} dR} dR\right\} , \tag{17}$$

or in an equivalent form:

$$\beta_1 = \frac{1}{\epsilon}\left\{\frac{P e^{-2\int_{R_c}^{R}\left(\frac{\eta\beta'_m}{\epsilon} - \alpha'_m\right)dR}}{\frac{P_c}{\beta'_{mc}+\epsilon_c\beta_{1c}} - 2\int_{R_c}^{R}\frac{\eta P}{\epsilon} e^{-2\int_{R_c}^{R}\left(\frac{\eta\beta'_m}{\epsilon} - \alpha'_m\right)dR} dR} - \beta'_m\right\} . \tag{18}$$

This solves the problem; β_2 can be derived from Eq.(6) and both aerosol extinction coefficients can be derived by applying the respective lidar ratioes: $\alpha_i = S_i\beta_i$. Note that

the considerations on mathematical stability of the solution by *Fernald* [1984] apply to this solution as well, and a far range calibration height with inward integration will yield much better results than a near range calibration with outward integration.

5. Application of the three-component method

Although cumbersome the above equations might seem, we have come up with a nice analytical solution that can be readily implemented in a computer program. Following the characterization described in section 3, we have chosen $S_1 = 82$ sr and $\delta_1 = 0.34$ to characterize the ash. The second aerosol type is the BL aerosol, which we will consider non-depolarising ($\delta_2 = 0$), as this appears reasonable from the volume depolarisation ratio plots in Fig. 1(b) and Fig. 2(b). Note that the assumption $\delta_2 = 0$ for BL aerosol does not have to be regarded as general for application of the method to measurements at other times or locations; a look at the volume depolarisation ratio time/height plot should however be able to give an indication in most conditions. For the BL aerosol, we also set a rural continental lidar ratio, $S_2 = 35$ sr, derived from the literature [*Browell et al.*, 1985].

As with some of the other lidar inversion techniques, we have to rely on a calibration portion of the atmosphere where we believe the profile to be purely molecular, and apply Eq. (3) and Eq. (16). To minimize the influence of shot-noise on the determination of K^* and K', we actually prefer choosing a calibration *range* rather than a single calibration *point*. We therefore modify our data inversion by calculating K^* and K' for each point in the calibration range (4500-5000 m in this work) and then averaging. R_c, i.e. the point from which integration is started, is chosen as the midpoint. It is worth mentioning that

we have found the solution to be more stable if both calibration ranges (used to determine K^* and K', respectively) are chosen identical.

Fig. 4 and 5 display the results in terms of extinction coefficient for ash and BL aerosols separately. We observe that the separation between the aerosol types is in general correct, and that the two aerosol types are dispatched quite well by the three-component method. The mixing of ash into the BL after 15:00 LT on 18 April is picked up very well, and on the same day the layer observed at 3500–4000 m also shows up in the panel displaying the ash extinction coefficient. Concerning the ash mixed in the BL, there would have been no possibility to quantify it with a traditional two-component approach (unless additional information were available) and it is in such a configuration that the three-component method displays its superiority.

6. Discussion and conclusions

We have developed a three-component atmosphere approach to the lidar equation, and have applied it to observations featuring, after cloud screening, a depolarising aerosol (ash) and a non-depolarising aerosol (BL aerosol). The three-component method showed to correctly resolve the two aerosol types and determine their individual contribution to the backscattering and extinction coefficients. The implication is the possibility of isolating the contribution of volcanic ash in lidar returns, and thus of quantifying it in terms of optical properties.

On 16 April, an apparent descent of the aerosol layer with time was observed from an altitude of $\sim$ 2800 m at 14:00 LT to $\sim$ 1400 m at 20:00 LT, when the layer was observed just above the BL aerosol. The average apparent descent rate over the observation period was thus $\sim$ 200 m/h, but as a matter of fact most of the descent happened between 16:00

and 17:00 LT, at a rate of $\sim$ 850 m/h, whereas both before and after that time range the rate was $\sim$ 100 m/h. The ash layer was also very narrow: its depth (full width half maximum, FWHM) was as little as $\sim$ 100 m before 16:00 LT, then increased to $\sim$ 400 m for an hour, and then decreased again to $\sim$ 150 m. It has to be remarked that the increased layer depth coincided with the faster apparent descent rate. The average and maximum aerosol optical depths (AOD) for the ash layer were 0.11 and 0.2, respectively, with a peak extinction coefficient (maximum of the vertical distribution, computed profile by profile) ranging 5–10$\cdot 10^{-4}$ m^{-1}.

On 18 April a double ash layer was observed between 10:00 and 14:00 LT between 1000 and 1500 m; its apparent descent rate was quite small compared to 16 April ($\sim$ 30 m/h) and the ash in fact gently sat just above the BL top until 15:00 LT. The depth of the ash layer (FWHM) was around $\sim$ 400 m; its peak extinction coefficient was 6–7$\cdot 10^{-4}$ m^{-1}, and its average and maximum optical depths were 0.19 and 0.27, respectively. After 14:00 LT, however, the BL depth increased as can be seen in Fig. 5(b), and the ash was entrained into its turbulent flow as shown in panel (a). The BL depth was $\sim$ 1400 m at 15:00–16:00 LT and it later increased up to 1700–1800 m; it is interesting to note that although the ash extinction coefficient decreased to $\sim 10^{-4}$ m^{-1}, the ash contribution to the AOD remained significant. As integrated from the lidar observations starting at a range of 300 m (overlap), the average and maximum AODs for this layer were 0.1 and 0.15, respectively (ash contribution only). Assuming a homogeneous vertical distribution from ground to 1500 m, we can estimate the ash AOD for the 0–300 m layer to be a fifth of the BL ash optical depth, and thus revise the above values by adding $\sim$ 25%. An

additional ash layer was observed on 18 April at 3500–4000 m; this layer was optically very thin (estimated AOD 0.02–0.04).

Mass concentration estimates, which is what is required for aviation and for modelling purposes, can be derived from extinction coefficient by application of an agreed value of the volcanic ash specific extinction. The proposed method can thus be considered a considerable advance into the objective of measuring volcanic ash concentrations by lidar. At the moment, existing estimates of the specific extinction for volcanic ash are as follows: 0.6 m^2/g (Ben Johnson, personal communication); 0.7 m^2/g [*Hogan et al.*, 2010] and 0.75 m^2/g [*Ansmann et al.*, 2010]. Volcanic ash particles can be considered "large" compared to visible wavelengths: a typical effective radius far from the source around $r \sim 1$ μm is equivalent to a Mie scattering size parameter $x = 2\pi r/\lambda \sim 10$ (for $\lambda \sim 550$ nm). As large particles usually present an Ångström exponent near zero (geometrical optics limit), we can consider that no significant spectral variation of the specific extinction has to be accounted for. As the ash extinction coefficient peaked 10^{-3} m^{-1} on April 16 and $7 \cdot 10^{-4}$ m^{-1} on April 18, we estimate the ash concentration to have peaked ~ 1500 and ~ 1000 $\mu g/m^3$, respectively. These concentrations can be retained as quite large when compared to the guidelines of 200, 2000 and 4000 $\mu g/m^3$ set by the civil aviation authorities.

Acknowledgments. Thanks to Joss Kent, Robert King and Paul Barrett for helping with the lidar operation.

References

Ansmann, A., M. Tesche, S. Groß, V. Freudenthaler, P. Seifert, A. Hiebsch, J. Schmidt, U. Wandinger, I. Mattis, D. Müller, and M. Wiegner (2010), The 16 april 2010 major volcanic ash plume over central Europe: EARLINET lidar and AERONET photometer observations at Leipzig and Munich, Germany, *Geophys. Res. Lett.*, L13810, doi:10.1029/2010GL043809.

Behrendt, A., and T. Nakamura (2002), Calculation of the calibration constant of polarization lidar and its dependency on atmospheric temperature, *Opt. Expr.*, *10*, 805–817.

Browell, E. V., S. Ismail, and S. T. Shipley (1985), Ultraviolet DIAL measurements of O3 profiles in regions of spatially inhomogeneous aerosols, *Appl. Opt.*, *24*, 2827–2836.

Di Girolamo, P., M. Cacciani, A. D. Sarra, G. Fiocco, and D. Fuà (1994), Lidar observations of the Pinatubo aerosol layer at Thule, Greenland, *Geophys. Res. Lett.*, *21*, 1295–1298.

Fernald, F. G. (1984), Analysis of atmospheric lidar observations: some comments, *Appl. Opt.*, *23*, 652–653.

Fernald, F. G., B. M. Herman, and J. A. Reagan (1972), Determination of aerosol height distribution by lidar, *J. Appl. Meteor.*, *11*, 482–489.

Flentje, H., H. Claude, T. Elste, S. Gilge, U. Köhler, C. Plass-Dülmer, W. Steinbrecht, W. Thomas, A. Werner, and W. Fricke (2010), The Eyiafjallajökull eruption in April 2010 — detection of volcanic plume using in-situ measurements, ozone sondes and a new generation ceilometer network, *Atmos. Chem. Phys. Discuss.*, *10*, 14,947–14,968.

Freudenthaler, V., M. Esselborn, M. Wiegner, B. Heese, M. Tesche, A. Ansmann, D. Müller, D. Althausen, M. Wirth, A. Fix, G. Ehret, P. Knippertz, C. Toledano,

J. Gasteiger, M. Garhammer, and M. Seefeldner (2009), Depolarization ratio profiling at several wavelengths in pure Saharan dust during SAMUM 2006, *Tellus*, *61B*, 165–179.

Gertisser, R. (2010), Eyjafjallajökull volcano causes widespread disruption to European air traffic, *Geol. Today*, *26*, 94–95.

Hogan, R. J., J. M. Haywood, H. F. Dacre, C. D. Westbrook, E. J. O'Connor, F. Marenco, C. L. Wrench, and S. E. Belcher (2010), Lidar and sun-photometer retrievals of ash particle size and mass concentration from the Eyjafjallajökull volcano, *To be submitted to J. Geophys. Res.*

Klett, J. D. (1985), Lidar inversion with variable backscatter/extinction ratios, *Appl. Opt.*, *24*, 1638–1643.

Kovalev, V. A. (1993), Lidar measurements of the vertical aerosol extinction profiles with range-dependent backscatter-to-extinction ratios, *Appl. Opt.*, *32*, 6053–6065.

Marenco, F., V. Santacesaria, A. F. Bais, D. Balis, A. di Sarra, A. Papayannis, and C. Zerefos (1997), Optical properties of tropospheric aerosols determined by lidar and spectrophotometric measurements (Photochemical Activity and Solar Ultraviolet Radiation campaign), *Appl. Opt.*, *36*, 6875–6886.

Mona, L., A. Amodeo, A. Boselli, C. Cornacchia, G. D'Amico, A. Giunta, F. Madonna, and G. Pappalardo (2010), Observations of the Eyjafjallajökull eruption's plume at Potenza EARLINET station, *Geophys. Res. Abs.*, *12*, EGU2010–15,747.

Petersen, G. N. (2010), A short meteorological overview of the Eyjafjallajökull eruption 14 April–23 May 2010, *Weather*, *65*, 203–207.

Pietruczuk, A., J. W. Krzyścin, J. Jaroslawski, J. Podgórski, P. Sobolewski, and J. Wink (2010), Eyjafjallajökull volcano ash observed over Belsk (52°N, 21°E), Poland, in April

2010, *Int. J. Remote Sensing*, *31*, 3981–3986.

Schumann, U., B. Weinzierl, O. Reitebuch, H. Schlager, A. Minikin, C. Forster, R. Baumann, T. Sailer, K. Graf, H. Mannstein, C. Voigt, S. Rahm, R. Simmet, M. Scheibe, M. Lichtenstern, P. Stock, H. Rüba, D. Schäuble, A. Tafferner, M. Rautenhaus, T. Gerz, H. Ziereis, M. Krautstrunk, C. Mallaun, J.-F. Gayet, K. Lieke, K. Kandler, M. Ebert, S. W. A. Stohl, J. Gasteiger, H. Olafsson, and K. Sturm (2010), Airborne observations of the Eyjafjalla volcano ash cloud over Europe during air space closure in April and May 2010, *Atmos. Chem. Phys. Discuss.*, *10*, 22,131–22,218.

Takamura, T., Y. Sasanu, and T. Hayasaka (1994), Tropospheric aerosol optical properties derived from lidar, sun photometer, and optical particle counter measurements, *Appl. Opt.*, *33*, 7132–7140.

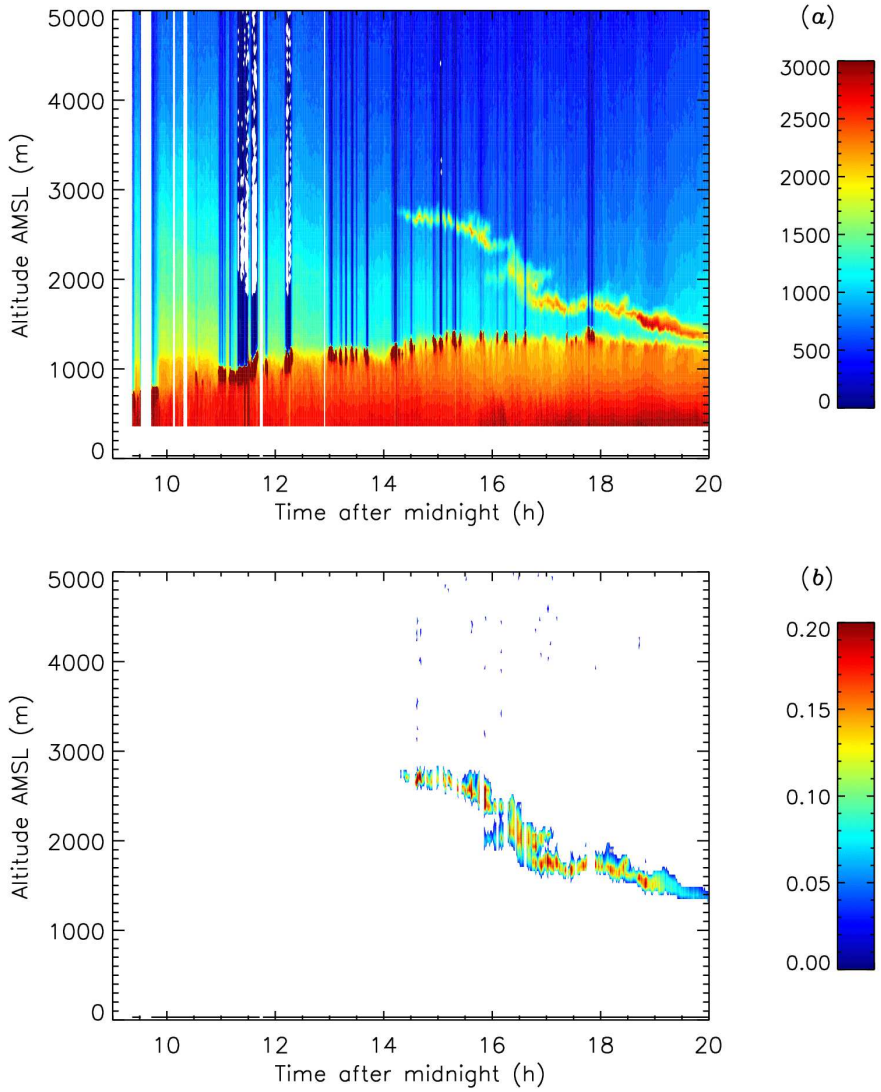

Figure 1. Lidar data for 16 April 2010 as a function of time (UTC+1) and altitude: (a) range corrected signal (arbitrary units) and (b) volume depolarisation ratio. For a better graphical rendering, volume depolarisation ratioes smaller than 0.02 are left out blank.

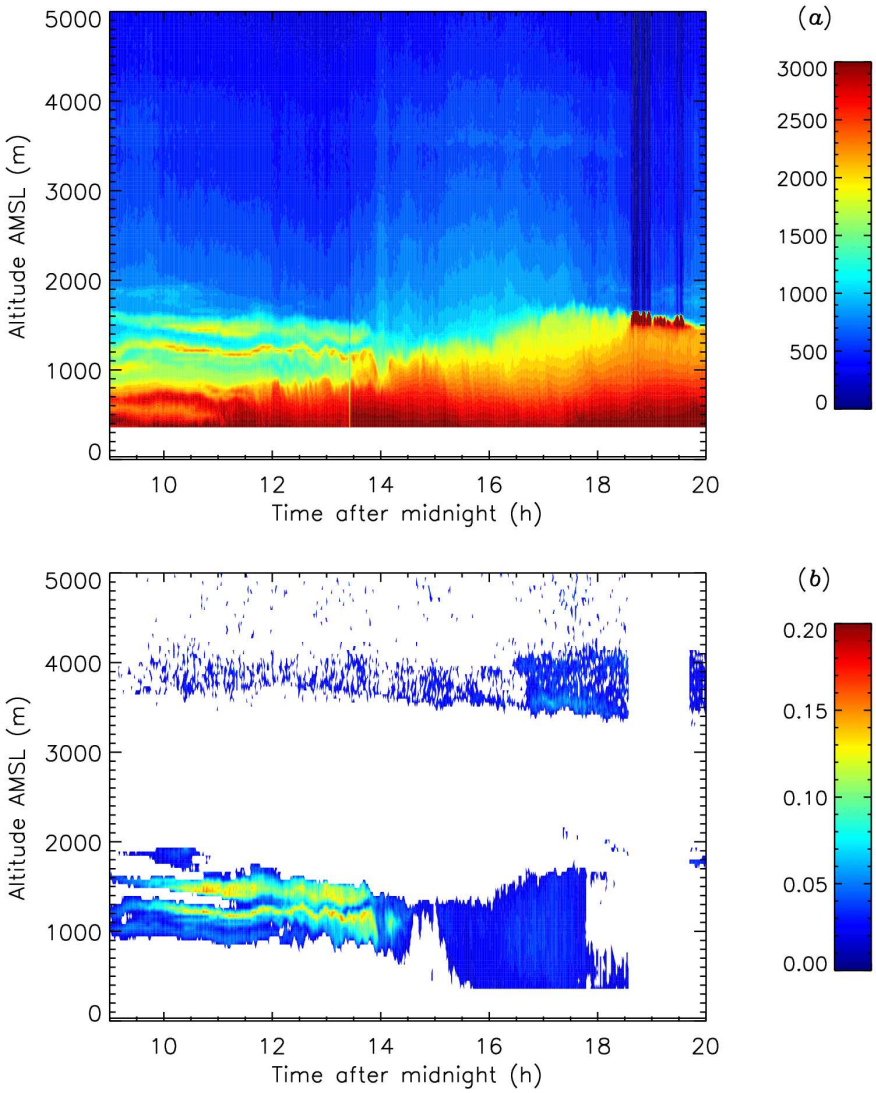

Figure 2. The same as Fig. 1, but for 18 April.

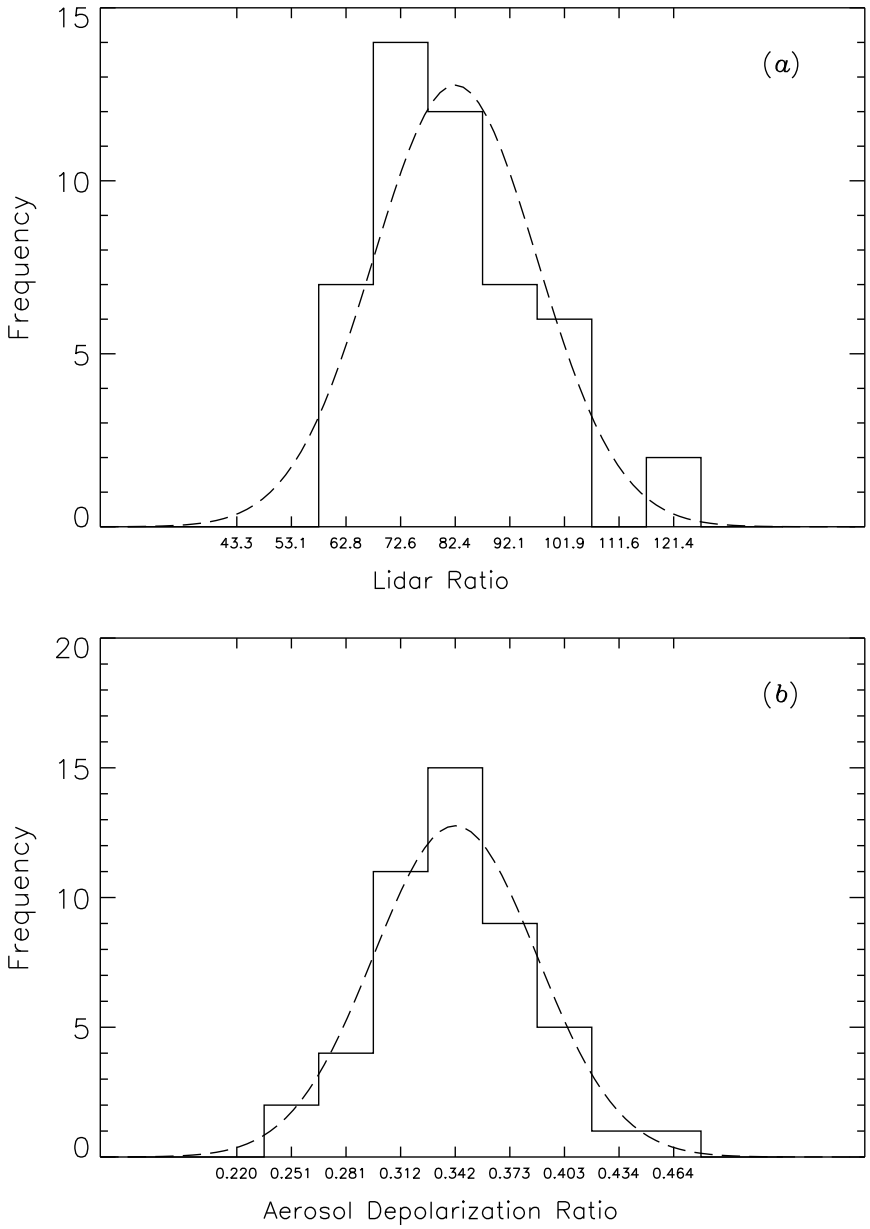

Figure 3. Lidar ratio (a) and aerosol depolarisation ratio (b) for the ash layer, as determined from 48 selected 5-min integration profiles (see text). A gaussian curve having the mean and standard deviation of the data sample is superimposed (dashed line).

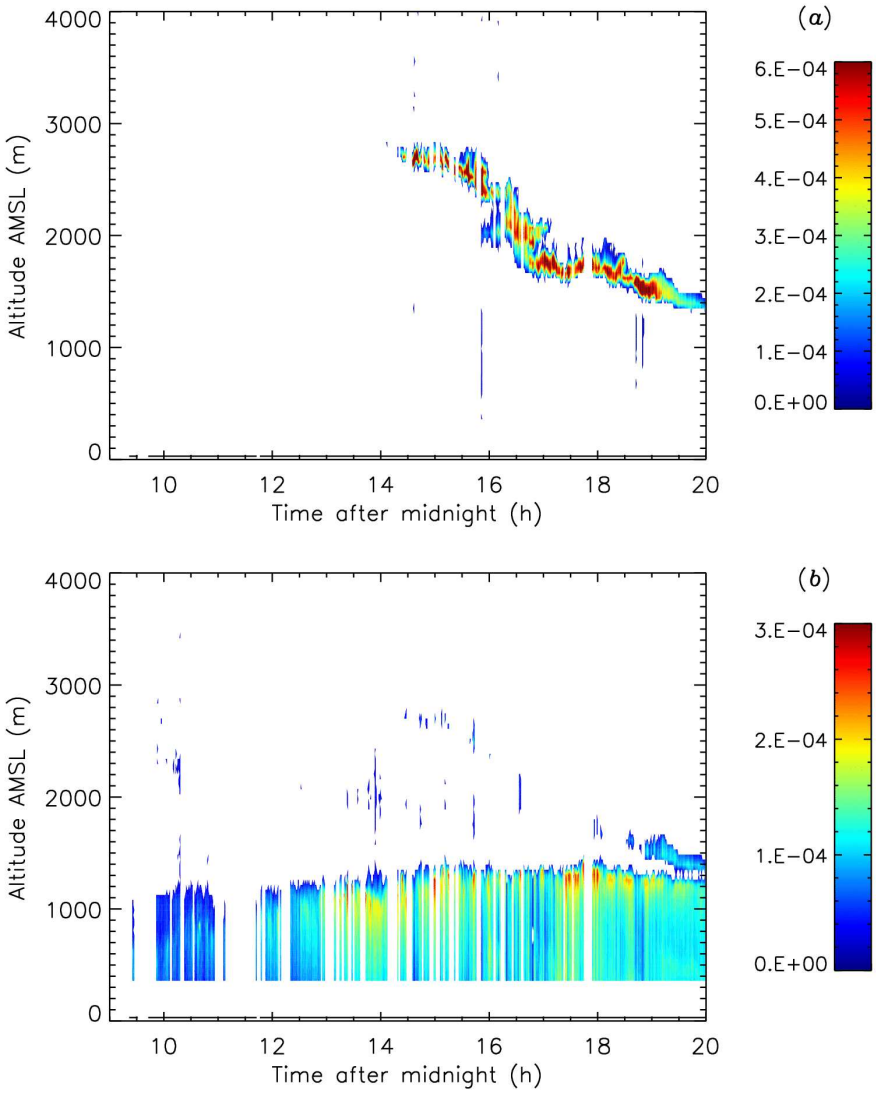

Figure 4. Ash aerosol extinction coefficient (a) and Boundary Layer aerosol extinction coefficient (b) for 16 April, as a result of the three-component atmosphere inversion method. Please note that different colour scales apply to panels (a) and (b). Units m^{-1}. For a better graphical rendering, extinction coefficients smaller than $2 \cdot 10^{-5}$ m^{-1} are left out blank.

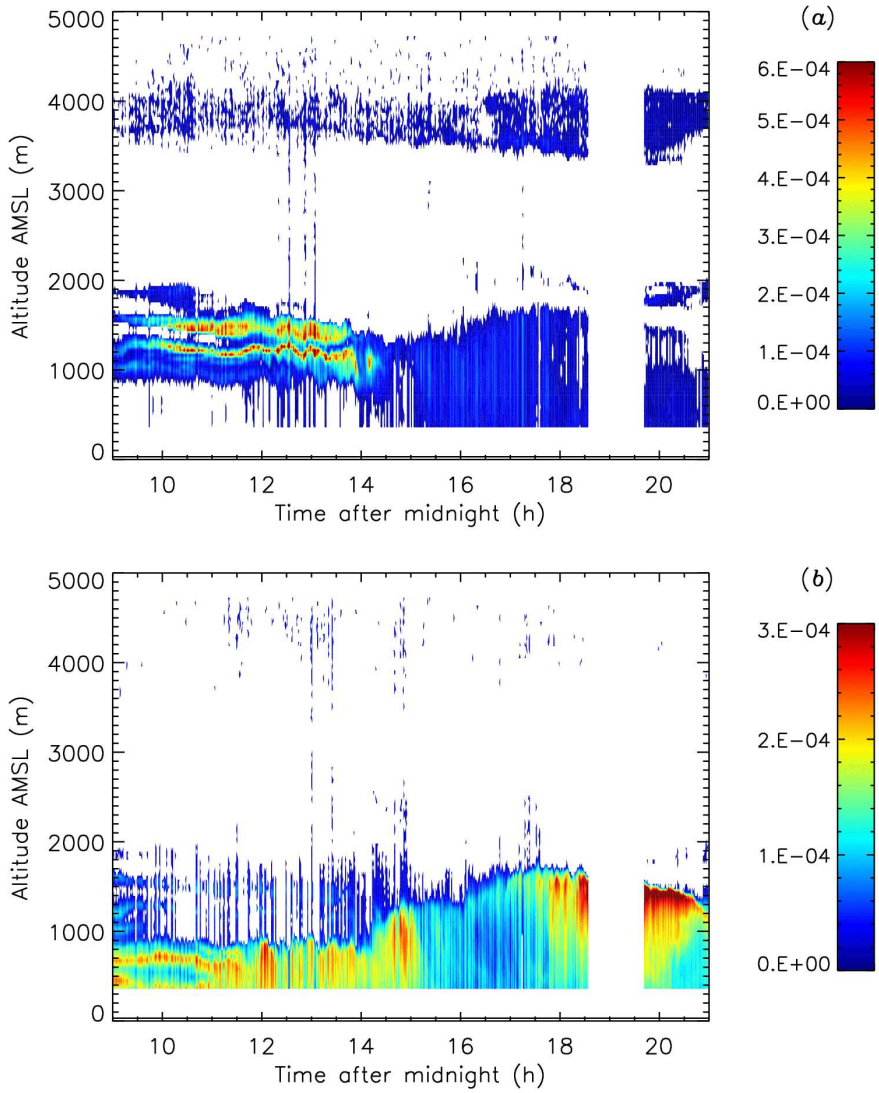

Figure 5. The same as Fig. 4, but for 18 April.